ACS OMEGA

http://pubs.acs.org/journal/acsodf Article

Epitaxial Growth of β-Ga_2O_3 Thin Films on Si with YSZ Buffer Layer

Hyung-Jin Choi, Jun Young Lee, Soo Young Jung, Ruiguang Ning, Min-Seok Kim, Sung-Jin Jung, Sung Ok Won, Seung-Hyub Baek,* and Ji-Soo Jang*

Cite This: ACS Omega 2022, 7, 43603−43608 Read Online

ABSTRACT: We report the epitaxial growth of ($\bar{2}01$)-oriented β-Ga_2O_3 thin films on a (001) Si substrate using the pulsed laser deposition technique employing epitaxial yttria-stabilized zirconia (YSZ) buffer layers. Epitaxial β-Ga_2O_3 thin films possess a biaxial compressive strain on YSZ single-crystal substrates while they exhibit a biaxial tensile strain on YSZ-buffered Si substrates. Post-annealing improves the crystalline quality of β-Ga_2O_3 thin films. High-resolution X-ray diffraction analyses reveal that the epitaxial ($\bar{2}01$) β-Ga_2O_3 thin films on Si have eight in-plane domain variants to accommodate the large difference in the crystal structure between monoclinic β-Ga_2O_3 and cubic YSZ. The results provide a pathway to integrate epitaxial β-Ga_2O_3 thin films on a Si gold standard substrate, which will expand the application scope beyond high-power electronics.

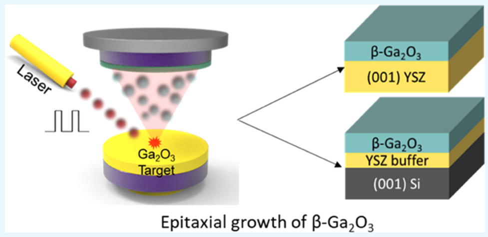

INTRODUCTION

Recently, Ga_2O_3 has attracted significant attention as a promising wide-bandgap semiconductor for applications in high-power devices, ultraviolet photodetectors, and gas sensors. Among the five Ga_2O_3 polymorphs (α, β, γ, δ, and ε), monoclinic β-Ga_2O_3 is the most thermodynamically stable and exhibits excellent physical properties, such as a wide band gap (~4.9 eV), optical transparency, n-type semiconducting properties, high electrical breakdown voltage (~8 MV/cm), and radiation resistance.[1−3]

The epitaxial growth of Ga_2O_3 thin films is important for the realization of high-performance devices and understanding their intrinsic properties. Thus far, many growth techniques have been reported for the epitaxial growth of Ga_2O_3 thin films, including pulsed laser deposition (PLD),[4,5] molecular beam epitaxy,[6] metal−organic chemical vapor deposition (CVD),[7] mist-CVD,[8] sol−gel,[9] and sputtering.[10] For high-power devices, homoepitaxial Ga_2O_3 structures, wherein both the film and substrate are β-Ga_2O_3, are desirable because a key feature of high-power electronics is a high resistance to electrical breakdown under high voltage conditions. Several fabrication techniques for β-Ga_2O_3 bulk single crystals have been developed, such as Verneuil,[11] floating,[12] Czochralski,[13] edge-defined film growth,[14] and vertical Bridgman methods.[15] However, β-Ga_2O_3 single-crystal substrates are very expensive compared to other single-crystal oxide and semiconductor substrates, which limits the application of homoepitaxial Ga_2O_3 structures. In addition, heteroepitaxial structures are formed when β-Ga_2O_3 thin films are grown on different substrates, such as MgO,[16] CeO_2,[17] and Al_2O_3.[18] These have also been widely studied.

In this study, we investigated the epitaxial growth of β-Ga_2O_3 thin films on Si substrates, the gold standard single crystal of modern electronics[19−21] using the PLD technique. ($\bar{2}01$)-Oriented epitaxial β-Ga_2O_3 thin films were grown on yttria-stabilized zirconia (YSZ) and YSZ-buffered Si substrates. Using high-resolution X-ray diffraction (HRXRD), we analyzed domain structures and strain states of monoclinic β-Ga_2O_3 thin films on cubic YSZ-buffered Si substrates and demonstrated the improved crystalline quality through a post-annealing process. The results provide a pathway for integrating the functionalities of β-Ga_2O_3 thin films onto Si, which can broaden the scope of β-Ga_2O_3 applications beyond high-power electronics.

RESULTS AND DISCUSSION

Figure 1a shows schematics of the β-Ga_2O_3, YSZ, and Si unit cells. YSZ has a fluorite structure ($Fm\bar{3}m$, cubic), with a lattice parameter of 5.143 Å. Owing to the small lattice mismatch with Si ($Fm\bar{3}m$, cubic, 5.431 Å), YSZ can be grown epitaxially on Si. The epitaxial YSZ layers on Si can function as a buffer layer to integrate additional functional oxide overlayers onto Si.[22−25] Owing to their unique growth process, involving the scavenging effect, epitaxial YSZ buffer layers can be deposited on Si using low-cost deposition processes, such as PLD and sputtering. β-Ga_2O_3 belongs to a monoclinic crystal system ($C2/m$, a = 12.23 Å, b = 3.04 Å, c = 5.80 Å, and β = 103.7°) and has a large lattice mismatch with cubic YSZ and Si substrates. Typically, complex

Received: July 13, 2022
Accepted: November 10, 2022
Published: November 24, 2022

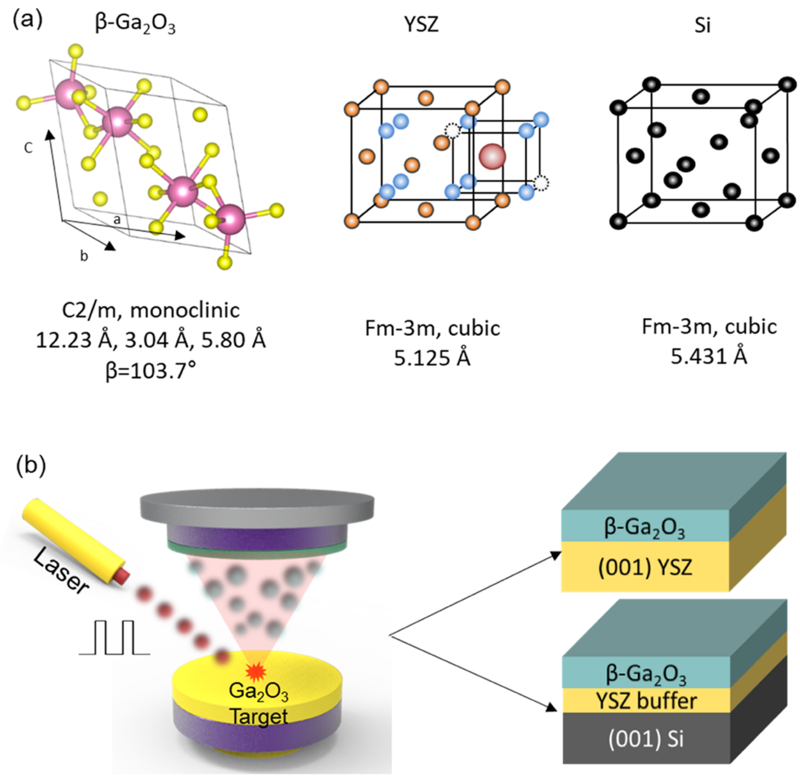

Figure 1. (a) Schematics of unit cells for β-Ga_2O_3, YSZ, and Si. (b) Schematic of the fabrication process of epitaxial β-Ga_2O_3 films on two types of substrates: (i) YSZ single-crystal and (ii) YSZ-buffered (001) Si substrates.

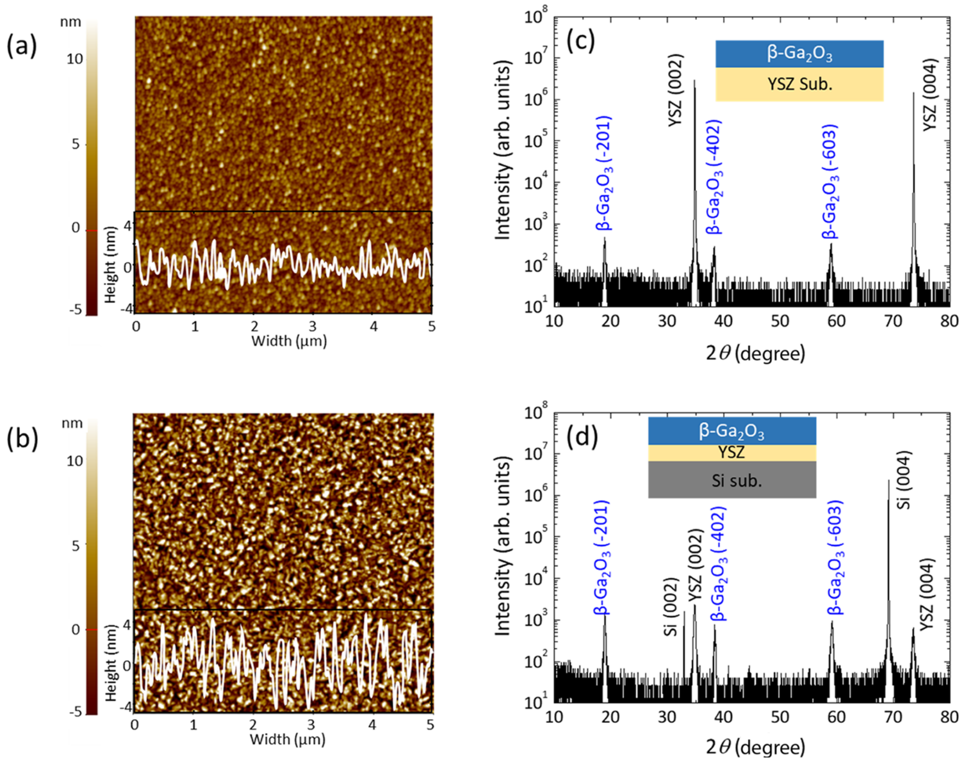

Figure 2. θ−2θ XRD pattern and surface morphologies measured via AFM of epitaxial β-Ga_2O_3 thin films on (a, c) YSZ and (b, d) YSZ-buffered Si substrates.

domain structures evolve when a material with low symmetry is epitaxially grown on a substrate with high symmetry; for example, epitaxial $BiFeO_3$ (rhombohedral) thin films have four structural variants on $SrTiO_3$ (cubic) substrates.[26] Therefore, it is expected that epitaxial β-Ga_2O_3 thin films on YSZ and YSZ-buffered Si substrates will exhibit a complex domain structure. In addition to the lattice mismatch, thermal mismatch affects epitaxial β-Ga_2O_3 thin films, particularly their strain state. A large

https://doi.org/10.1021/acsomega.2c04387
ACS Omega 2022, 7, 43603−43608

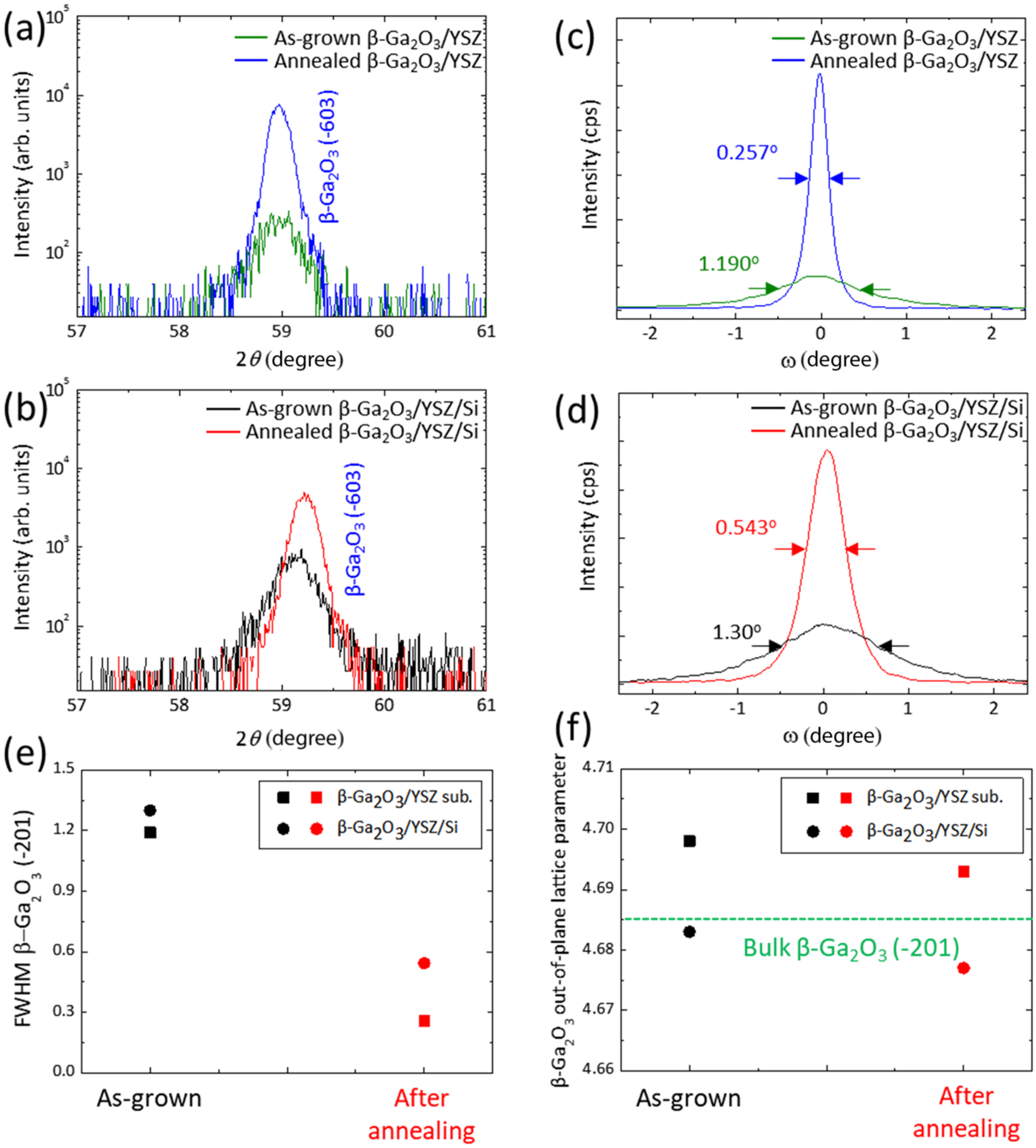

Figure 3. (a) β-Ga_2O_3 ($\bar{2}01$) θ−2θ XRD pattern of the as-grown and annealed β-Ga_2O_3 on the YSZ substrate. (b) β-Ga_2O_3 ($\bar{2}01$) θ-2θ XRD pattern of the as-grown and annealed β-Ga_2O_3 on the YSZ-buffered Si substrate. (c) Rocking curve of Ga_2O_3($\bar{2}01$) peaks for as-grown and annealed β-Ga_2O_3 on the YSZ substrate. (d) Rocking curve of β-Ga_2O_3($\bar{2}01$) peaks for as-grown and annealed β-Ga_2O_3 on the YSZ-buffered Si substrate. (e) FWHM values of the ($\bar{2}01$) plane of the as-grown and annealed β-Ga_2O_3 thin films. (f) Out-of-plane lattice parameter of the ($\bar{2}01$) plane of the as-grown and annealed β-Ga_2O_3 thin films.

difference exists in the thermal expansion coefficients of β-Ga_2O_3 ($\sim 5 \times 10^{-6}$/K), YSZ ($\sim 9 \times 10^{-6}$/K), and Si ($\sim 3 \times 10^{-6}$/K). Typically, epitaxial oxide thin films grown on Si possess tensile strain at room temperature because of the thermal mismatch due to cooling to room temperature. To study this effect, we grew epitaxial β-Ga_2O_3 thin films on both YSZ and YSZ-buffered Si substrates via PLD, as shown in Figure 1b.

β-Ga_2O_3 thin films were grown via PLD using a KrF excimer laser (λ = 248 nm) at 100 mTorr O_2 partial pressure with a laser energy density of 1.5 J/cm^2 and frequency of 5 Hz at 750 °C. A Ga_2O_3 ceramic target was used with a sample-to-target distance of 5 cm. Epitaxial β-Ga_2O_3 thin films were grown on two different substrates: (001) YSZ and YSZ-buffered (001) Si single-crystal (YSZ-buffered Si) substrates. A 45 nm-thick epitaxial YSZ buffer layer was grown via PLD at 0.1 mTorr O_2 partial pressure with a laser energy density of 1.5 J/cm^2 and frequency of 5 Hz at 750 °C. Note that the 45 nm-thick epitaxial YSZ buffer layer was selected considering the crystallinity of each thickness sample (Figure S2). A YSZ ceramic target with a composition of 20%Y-ZrO_2 was used with a sample-to-target distance of 5 cm. The growth rate was maintained at 6 nm/min. Before Ga_2O_3 deposition, both the YSZ and YSZ-buffered Si substrates were cleaned with acetone, isopropyl alcohol, and DI water, followed by N_2 drying.

Commercial atomic force microscopy (AFM, Digital Instrument Dimension 3100, equipped with a Nanoscope IV controller) was used to investigate the surface morphology of β-Ga_2O_3 thin films in the tapping mode. Figure 2a,b show AFM

https://doi.org/10.1021/acsomega.2c04387
ACS Omega 2022, 7, 43603−43608

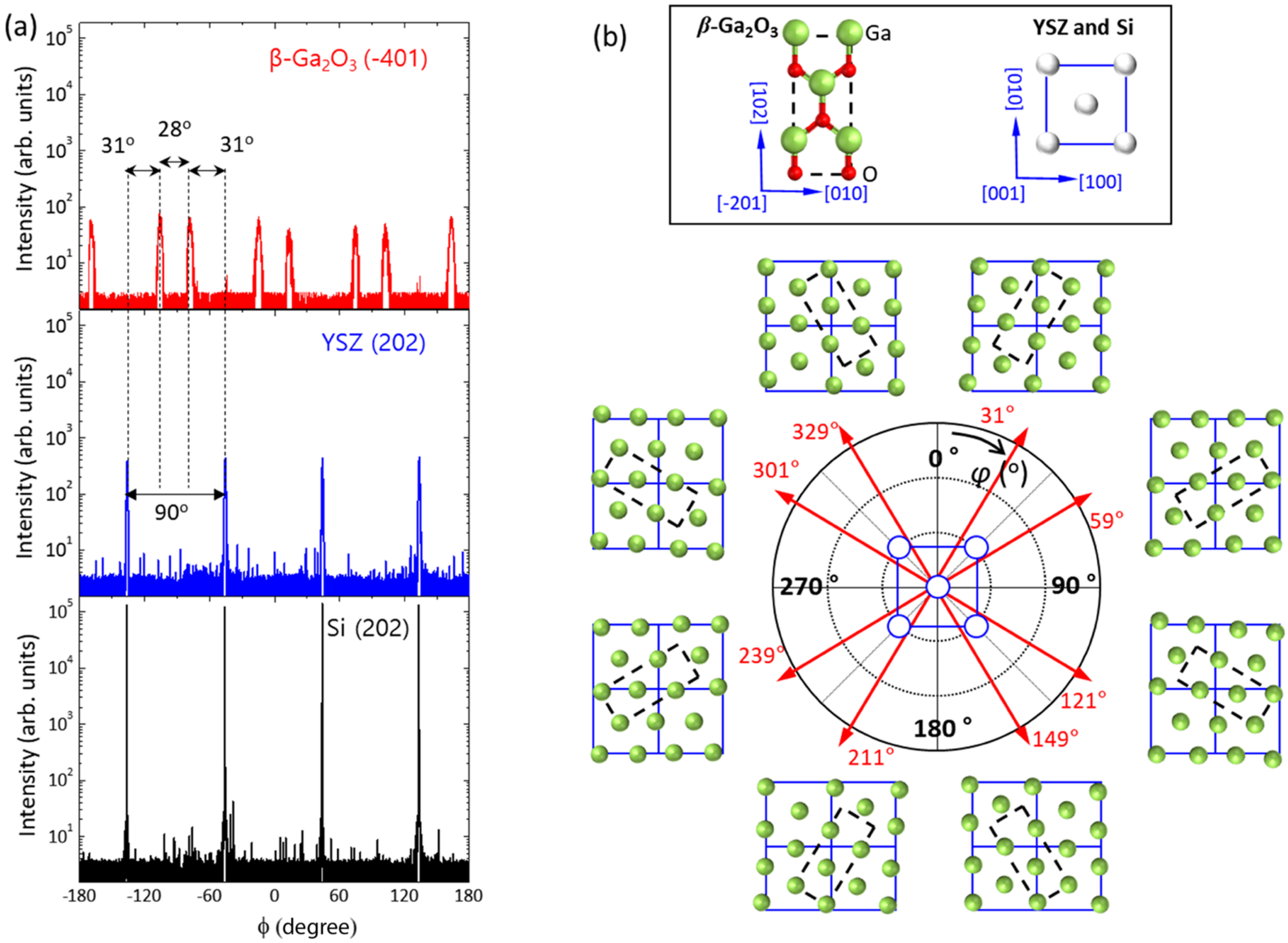

Figure 4. (a) φ-scan of β-$Ga_2O_3(\bar{4}01)$ plane (red), YSZ (202) plane (blue), and Si(202) plane (black) of β-Ga_2O_3 on the YSZ-buffered Si substrate. (b) Schematic of epitaxial relationship between YSZ (001) plane and β-$Ga_2O_3(\bar{2}01)$ plane.

images of β-Ga_2O_3 thin films grown on YSZ and YSZ-buffered Si substrates, respectively. The β-Ga_2O_3 film on the YSZ substrate exhibited a smooth surface with a height variation of ±2 nm. In contrast, the β-Ga_2O_3 film on YSZ-buffered Si substrates exhibited a slightly rougher surface with a height variation of ±4 nm. These results are also supported by SEM results (see Figure S1).

A high-resolution X-ray diffractometer (Bruker Discovery D8) equipped with a two-channel cut Ge(220) and four crystal monochromators (λ = 1.5406 Å, 30 kV) was used for the structural analysis of the epitaxial β-Ga_2O_3 thin films. Figure 2c,d show the XRD θ−2θ scan spectra of the β-Ga_2O_3 thin films deposited on YSZ and YSZ-buffered Si substrates, respectively. In both cases, the XRD θ−2θ patterns show only $\{\bar{2}01\}$ diffraction peaks. These results clearly indicate that both β-Ga_2O_3 thin films grown on the YSZ and YSZ-buffered Si substrates are epitaxially grown with a $(\bar{2}01)$ orientation along the out-of-plane direction.

To study the effect of thermal treatment on the crystalline quality and strain states of β-Ga_2O_3 thin films, we performed post-annealing processes. The samples were annealed in a tube furnace at 1100 °C under O_2 flow (20 sccm) for 5 h at a heating and cooling rate of ∼1 °C/min. This annealing condition did not cause cracks in β-Ga_2O_3 films. To evaluate the crystalline quality of the β-Ga_2O_3 films, we measured the full width at half maximum (FWHM) of the XRD rocking curve of the $(\bar{2}01)$ peak, which is the most intense peak. The strain states of β-Ga_2O_3 thin films were characterized by a shift in the $(\bar{6}03)$ diffraction peak. Figure 3a,b show the XRD θ−2θ scan (57−61°) of the β-Ga_2O_3 thin films deposited on the YSZ and YSZ-buffered Si substrates, respectively, before and after annealing. For both cases, the $(\bar{6}03)$ diffraction peak intensity increased by approximately one order of magnitude owing to thermal annealing, which indicates an improvement in the crystalline quality. The FWHMs of the $(\bar{2}01)$ rocking curves of β-Ga_2O_3 thin films deposited on the YSZ and YSZ-buffered Si substrates also increased from 1.190 to 0.257° (Figure 3c) and from 1.300 to 0.543° (Figure 3d), respectively, owing to thermal annealing. This indicates that the crystalline quality of β-Ga_2O_3 thin films on YSZ substrates is significantly improved through thermal annealing, as shown in Figure 3e.

Notably, the $(\bar{6}03)$ peak position in the θ−2θ scan of β-Ga_2O_3 thin films on YSZ-buffered Si substrates is higher than that of β-Ga_2O_3 thin films on YSZ substrates. Moreover, after thermal annealing, the peak of β-Ga_2O_3 thin films on the YSZ-buffered Si substrate shifted toward a higher angle, which indicates that the out-of-plane lattice parameter became smaller owing to thermal annealing. These results, summarized in Figure 3f, originate from the thermal stress that evolves from the difference in thermal expansion coefficients of β-Ga_2O_3 and Si.

To investigate the in-plane epitaxial relationship between a β-Ga_2O_3 thin film, YSZ buffer layer, and Si substrate, we

https://doi.org/10.1021/acsomega.2c04387
ACS Omega 2022, 7, 43603−43608

performed XRD azimuthal φ scans of β-$Ga_2O_3(\bar{4}01)$, YSZ (202), and Si(202) peaks, respectively, as shown in Figure 4a. For YSZ and Si, four peaks appear at the same φ angles at 90° intervals, indicating in-plane epitaxy with a cube-on-cube epitaxial relationship between the YSZ buffer layer and Si substrate. In contrast, eight β-$Ga_2O_3(\bar{4}01)$ diffraction peaks appeared at two distinct intervals of 31 and 28°. Note that the $(\bar{4}01)$ plane is unique without family planes in the monoclinic crystal structure. Therefore, one $(\bar{4}01)$ peak in the φ scan represents a particular domain of β-Ga_2O_3. Therefore, epitaxial β-Ga_2O_3 thin films on YSZ-buffered Si substrates had eight domain variants (Figure 4b). With respect to each of the four {100} directions of the YSZ-buffered Si unitcell, two domains exist, with the [102] direction of β-Ga_2O_3 rotated by ±31°. Based on the XRD results, all eight domains are summarized in Figure 4b. This complex domain structure is attributed to the large mismatch between crystal structures of β-Ga_2O_3 and YSZ. As a potential application of the β-Ga_2O_3 films, we carried out photo current test. As shown in Figure S3, the β-Ga_2O_3 films on interdigitated electrode clearly showed photo-resistive characteristics which can be potentially applied to photodetector.

In summary, we successfully grew $(\bar{2}01)$-oriented epitaxial β-Ga_2O_3 thin films on Si substrates by employing epitaxial YSZ buffer layers. Biaxial compressive strain evolved in the β-Ga_2O_3 thin films on the YSZ substrate, whereas biaxial tensile strain evolved in the β-Ga_2O_3 thin films on the YSZ-buffered Si substrate. To further improve the crystalline quality, post-annealing was performed. Finally, we reveal that epitaxial β-Ga_2O_3 thin films have a complex domain structure with eight domain variants. These results will provide a pathway to integrate epitaxial β-Ga_2O_3 thin films on Si, which can broaden the scope of β-Ga_2O_3 applications beyond high-power electronics and toward UV photodetectors and gas sensors.

■ ASSOCIATED CONTENT

Supporting Information

The Supporting Information is available free of charge at https://pubs.acs.org/doi/10.1021/acsomega.2c04387.

Additional experimental results, including SEM, FWHM, and photo-detector data (PDF)

■ AUTHOR INFORMATION

Corresponding Authors

Seung-Hyub Baek − *Electronic Materials Research Center, Korea Institute of Science and Technology, Seoul 02792, Republic of Korea; Division of Nano & Information Technology, KIST School, Korea University of Science and Technology, Seoul 02792, Republic of Korea; Department of Materials Science and Engineering, Yonsei University, Seoul 03722, Republic of Korea; Yonsei-KIST Convergence Research Institute, Korea Institute of Science and Technology, Seoul 02792, Republic of Korea*; Email: shbaek77@kist.re.kr

Ji-Soo Jang − *Electronic Materials Research Center, Korea Institute of Science and Technology, Seoul 02792, Republic of Korea*; orcid.org/0000-0001-6018-7231; Email: wkdwltn92@kist.re.kr

Authors

Hyung-Jin Choi − *Electronic Materials Research Center, Korea Institute of Science and Technology, Seoul 02792, Republic of Korea*

Jun Young Lee − *Electronic Materials Research Center, Korea Institute of Science and Technology, Seoul 02792, Republic of Korea*

Soo Young Jung − *Electronic Materials Research Center, Korea Institute of Science and Technology, Seoul 02792, Republic of Korea; Department of Materials Science and Engineering, Seoul National University (SNU), Seoul 08826, Republic of Korea*

Ruiguang Ning − *Electronic Materials Research Center, Korea Institute of Science and Technology, Seoul 02792, Republic of Korea; Division of Nano & Information Technology, KIST School, Korea University of Science and Technology, Seoul 02792, Republic of Korea*

Min-Seok Kim − *Electronic Materials Research Center, Korea Institute of Science and Technology, Seoul 02792, Republic of Korea; Department of Materials Science and Engineering, Research Institute of Advanced Materials, Seoul National University, Seoul 08826, Republic of Korea*

Sung-Jin Jung − *Electronic Materials Research Center, Korea Institute of Science and Technology, Seoul 02792, Republic of Korea*

Sung Ok Won − *Advanced Analysis Center, Korea Institute of Science and Technology, Seoul 02792, Republic of Korea*

Complete contact information is available at: https://pubs.acs.org/10.1021/acsomega.2c04387

Notes

The authors declare no competing financial interest.

■ ACKNOWLEDGMENTS

The authors gratefully acknowledge the financial support from the National Research Foundation of Korea (NRF) Grant funded by the Ministry of Science and ICT (NRF 2020M3F3A2A01081572 and NRF-2020M3D1A2101933). This work was supported by the Technology Innovation Program (00144157, Development of Heterogeneous Multi-Sensor Micro-System Platform) funded By the Ministry of Trade, Industry & Energy (MOTIE, Korea).

■ REFERENCES

(1) Pearton, S. J.; Yang, J.; Cary, P. H.; Ren, F.; Kim, J.; Tadjer, M. J.; Mastro, M. A. A review of Ga_2O_3 materials, processing, and devices. *Appl. Phys. Rev.* **2018**, *5*, No. 011301.

(2) Tak, B. R.; Kumar, S.; Kapoor, A. K.; Wang, D.; Li, X.; Sun, H.; Singh, R. Recent advances in the growth of gallium oxide thin films employing various growth techniques-a review. *J. Phys. D: Appl. Phys.* **2021**, *54*, No. 453002.

(3) Yao, Y.; Okur, S.; Lyle, L. A. M.; Tompa, G. S.; Salagaj, T.; Sbrockey, N.; Davis, R. F.; Porter, L. M. Growth and characterization of α-, β-, and ε-phases of Ga_2O_3 using MOCVD and HVPE techniques. *Mater. Res. Lett.* **2018**, *6*, 268−275.

(4) Leedy, K. D.; Chabak, K. D.; Vasilyev, V.; Look, D. C.; Boeckl, J. J.; Brown, J. L.; Tetlak, S. E.; Green, A. J.; Moser, N. A.; Crespo, A.; Thomson, D. B.; Fitch, R. C.; McCandless, J. P.; Jessen, G. H. Highly conductive homoepitaxial Si-doped Ga_2O_3 films on (010) β-Ga_2O_3 by pulsed laser deposition. *Appl. Phys. Lett.* **2017**, *111*, No. 012103.

(5) Zhang, F.; Arita, M.; Wang, X.; Chen, Z.; Saito, K.; Tanaka, T.; Nishio, M.; Motooka, T.; Guo, Q. Toward controlling the carrier density of Si doped Ga_2O_3 films by pulsed laser deposition. *Appl. Phys. Lett.* **2016**, *109*, No. 102105.

(6) Ghose, S.; Rahman, S.; Hong, L.; Rojas-Ramirez, J. S.; Jin, H.; Park, K.; Klie, R.; Droopad, R. Growth and characterization of β-Ga_2O_3 thin films by molecular beam epitaxy for deep-UV photodetectors. *J. Appl. Phys.* **2017**, *122*, No. 095302.

(7) Chen, Y.; Liang, H.; Xia, X.; Tao, P.; Shen, R.; Liu, Y.; Feng, Y.; Zheng, Y.; Li, X.; Du, G. The lattice distortion of β-Ga_2O_3 film grown on c-plane sapphire. *J. Mater. Sci.: Mater. Electron.* **2015**, *26*, 3231−3235.

(8) Nishinaka, H.; Tahara, D.; Yoshimoto, M. Heteroepitaxial growth of ε-Ga_2O_3thin films on cubic (111) MgO and (111) yttria-stablized zirconia substrates by mist chemical vapor deposition. *Jpn. J. Appl. Phys.* **2016**, *55*, No. 1202BC.

(9) Zhu, Y.; Xiu, X.; Cheng, F.; Li, Y.; Xie, Z.; Tao, T.; Chen, P.; Liu, B.; Zhang, R.; Zheng, Y.-D. Growth and nitridation of β-Ga_2O_3 thin films by Sol-Gel spin-coating epitaxy with post-annealing process. *J. Sol−Gel Sci. Technol.* **2021**, *100*, 183−191.

(10) Li, S.; Jiao, S.; Wang, D.; Gao, S.; Wang, J. The influence of sputtering power on the structural, morphological and optical properties of β-Ga_2O_3 thin films. *J. Alloys Compd.* **2018**, *753*, 186−191.

(11) Chase, A. O. Growth of b-Ga,O, by the Verneuil Technique. *J. Am. Ceram. Soc.* **1964**, *47*, No. 470.

(12) Víllora, E. G.; Shimamura, K.; Yoshikawa, Y.; Aoki, K.; Ichinose, N. Large-size β-Ga_2O_3 single crystals and wafers. *J. Cryst. Growth* **2004**, *270*, 420−426.

(13) Galazka, Z. Growth of bulk β-Ga_2O_3 single crystals by the Czochralski method. *J. Appl. Phys.* **2022**, *131*, No. 031103.

(14) Kuramata, A.; Koshi, K.; Watanabe, S.; Yamaoka, Y.; Masui, T.; Yamakoshi, S. High-quality β-Ga_2O_3 single crystals grown by edge-defined film-fed growth. *Jpn. J. Appl. Phys.* **2016**, *55*, No. 1202A2.

(15) Hoshikawa, K.; Ohba, E.; Kobayashi, T.; Yanagisawa, J.; Miyagawa, C.; Nakamura, Y. Growth of β-Ga_2O_3 single crystals using vertical Bridgman method in ambient air. *J. Cryst. Growth* **2016**, *447*, 36−41.

(16) Wakabayashi, R.; Yoshimatsu, K.; Hattori, M.; Ohtomo, A. Epitaxial structure and electronic property of β-Ga_2O_3 films grown on MgO (100) substrates by pulsed-laser deposition. *Appl. Phys. Rev.* **2017**, *111*, No. 162101.

(17) Tang, X.; Li, K. H.; Zhao, Y.; Sui, Y.; Liang, H.; Liu, Z.; Liao, C. H.; Babatain, W.; Lin, R.; Wang, C.; Lu, Y.; Alqatari, F. S.; Mei, Z.; Tang, W.; Li, X. Quasi-Epitaxial Growth of beta-Ga_2O_3-Coated Wide Band Gap Semiconductor Tape for Flexible UV Photodetectors. *ACS Appl. Mater. Interfaces* **2022**, *14*, 1304−1314.

(18) Li, Y.; Xiu, X.; Xu, W.; Zhang, L.; Xie, Z.; Tao, T.; Chen, P.; Liu, B.; Zhang, R.; Zheng, Y. Microstructural analysis of heteroepitaxial β-Ga_2O_3 films grown on (0001) sapphire by halide vapor phase epitaxy. *J. Phys. D: Appl. Phys.* **2020**, *54*, No. 014003.

(19) Baek, S. H.; Eom, C.-B. Epitaxial integration of perovskite-based multifunctional oxides on silicon. *Acta Mater.* **2013**, *61*, 2734−2750.

(20) Baek, S. H.; Park, J.; Kim, D. M.; Aksyuk, V. A.; Das, R. R.; Bu, S. D.; Felker, D. A.; Lettieri, J.; Vaithyanathan, V.; Bharadwaja, S. S. N.; Bassiri-Gharb, N.; Chen, Y. B.; Sun, H. P.; Folkman, C. M.; Jang, H. W.; Kreft, D. J.; Streiffer, S. K.; Ramesh, R.; Pan, X. Q.; Trolier-McKinstry, S.; Schlom, D. G.; Rzchowski, M. S.; Blick, R. H.; Eom, C. B. Giant Piezoelectricity on Si for Hyperactive MEMS. *Science* **2011**, *334*, 958−961.

(21) Lyu, J.; Fina, I.; Fontcuberta, J.; Sanchez, F. Epitaxial Integration on Si(001) of Ferroelectric $Hf_{0.5}Zr_{0.5}O_2$ Capacitors with High Retention and Endurance. *ACS Appl. Mater. Interfaces* **2019**, *11*, 6224−6229.

(22) Jun, S.; Kim, Y. S.; Lee, J.; Kim, Y. W. Dielectric properties of strained (Ba, Sr)TiO_3 thin films epitaxially grown on Si with thin yttria-stabilized zirconia buffer layer. *Appl. Phys. Lett.* **2001**, *78*, 2542−2544.

(23) Choi, H. J.; Jang, J.; Jung, S. Y.; Ning, R.; Kim, M. S.; Jung, S. J.; Lee, J. Y.; Park, J. S.; Lee, B. C.; Jang, J. S.; Kim, S. K.; Lee, K. H.; Lee, J. H.; Won, S. O.; Li, Y.; Hu, S.; Choi, S. Y.; Baek, S. H. Thermal stress-assisted annealing to improve the crystalline quality of epitaxial YSZ buffer layer on Si. *J. Mater. Chem. C* **2022**, *10*, 10027−10036.

(24) Dubbink, D.; Koster, G.; Rijnders, G. Growth mechanism of epitaxial YSZ on Si by Pulsed Laser Deposition. *Sci. Rep.* **2018**, *8*, No. 5774.

(25) Fukumoto, H.; Imura, T.; Osaka, Y. Heteroepitaxial growth of yttria-stabilized zirconia (YSZ) on silicon. *Jpn. J. Appl. Phys.* **1988**, *27*, No. L1404.

(26) Baek, S. H.; Jang, H. W.; Folkman, C. M.; Li, Y. L.; Winchester, B.; Zhang, J. X.; He, Q.; Chu, Y. H.; Nelson, C. T.; Rzchowski, M. S.; Pan, X. Q.; Ramesh, R.; Chen, L. Q.; Eom, C. B. Ferroelastic switching for nanoscale non-volatile magnetoelectric devices. *Nat. Mater.* **2010**, *9*, 309−314.

https://doi.org/10.1021/acsomega.2c04387
ACS Omega 2022, 7, 43603−43608